INSTITUTE OF PHYSICS PUBLISHING JOURNAL OF PHYSICS: CONDENSED MATTER

J. Phys.: Condens. Matter **14** (2002) 5497–5516 PII: S0953-8984(02)33074-1

First-principles energy and stress fields in defected materials

R Ramprasad

Semiconductor Products Sector, Motorola, Inc., 2100 E. Elliot Road, Tempe, AZ 85284, USA

Received 28 January 2002
Published 23 May 2002
Online at stacks.iop.org/JPhysCM/14/5497

Abstract

New methods are presented for microscopically characterizing defects in materials in terms of local energy and stress fields calculated at the first-principles level of theory. These fields provide a quantitative measure of the local disturbance created by defect-induced electronic and atomic inhomogeneities in a solid. The local stress density $\sigma_{\alpha\beta}(\boldsymbol{r})$ is computed by explicitly evaluating the strain derivative of a suitably defined energy density field, $\varepsilon(\boldsymbol{r})$. Although $\varepsilon(\boldsymbol{r})$ and $\sigma_{\alpha\beta}(\boldsymbol{r})$ are defined only up to a gauge transformation, they yield the correct total energy and the average macroscopic stress tensor, respectively, when integrated over the entire volume of the underlying unit cell. In systems with defects, it is shown that well-defined averages of $\varepsilon(\boldsymbol{r})$ and $\sigma_{\alpha\beta}(\boldsymbol{r})$ can be constructed by restricting the domain of integration to smaller volumes, which are integral multiples of the Wigner–Seitz cell for the supercell containing the defect. These fields can provide important insights into the nature of atomic-scale defects. Explicit expressions for $\varepsilon(\boldsymbol{r})$ and $\sigma_{\alpha\beta}(\boldsymbol{r})$ are derived within the density functional plane-wave pseudopotential formalism. For the test cases of bulk Al with a vacancy and a Al(001) surface, it is shown that the averaged forms of $\varepsilon(\boldsymbol{r})$ and $\sigma_{\alpha\beta}(\boldsymbol{r})$ help characterize the defects in a physically meaningful manner. Potential applications of $\varepsilon(\boldsymbol{r})$ and $\sigma_{\alpha\beta}(\boldsymbol{r})$ to the characterization of surface relaxations and to multi-scale studies of materials are suggested.

1. Introduction

Defects, and their dynamics, play a crucial role in determining mechanical and diffusion-dominated materials properties. Since the local chemistry and coordination environment at a defect are vastly different from those in the defect-free bulk region of the material, a detailed, microscopic analysis of key properties in the vicinity of the defect is essential to understanding observed macroscopic materials behaviour.

In traditional electronic structure calculations, periodic supercells are frequently used to study defects. The supercell contains the defect and sufficient surrounding bulk material so that

the defect is well separated from its periodic images. A characteristic feature of such supercell methods is that they result in quantities that are properties of the supercell as a whole—e.g., the total energy and the average macroscopic stress. There is thus an emphasis on a *global* description, with individual contributions from different parts of the material becoming inextricably combined in the calculated global quantities. The purpose of this study is to introduce new analysis tools within the framework of electronic structure supercell methods to enable a microscopic characterization of the inhomogeneities at defects in periodic solid-state systems. These methods lead to a decomposition of the integrated global quantities into spatially varying fields. We show that the resulting fields, when re-integrated over appropriate volumes within the supercell, effectively capture those features specific to a defect, yielding a detailed local picture of the defect.

Recently, Chetty and Martin [1] introduced the concept of a spatially varying energy density field, $\varepsilon(\boldsymbol{r})$, which is local in real space, and whose integral over the volume of the supercell is the total energy per supercell. Since the total energy within the pseudopotential formalism is itself comprised of separate contributions, some of which are non-local in nature [2], and since $\varepsilon(\boldsymbol{r})$ can be defined only up to an additive scalar field (which itself integrates to zero within the supercell), there is an inherent non-uniqueness associated with any such form of the local energy density. Thus, while the integral of $\varepsilon(\boldsymbol{r})$ over the volume of the entire supercell is a well-defined quantity, its integral over parts of the supercell is, in general, ill-defined. Despite this non-uniqueness problem, Chetty and Martin [1, 3] showed that one can arrive at physically meaningful results by integrating the local energy density over a portion of the supercell, specifically the surface region. They demonstrated that the local energy density helps partition space into a surface region and a bulk region, with the energy density deviating from its bulk value in the surface region in an understandable manner. In the present study, we extend the approach of Chetty and Martin [1] from surfaces to more general defects, and make a formal identification of those parts of the supercell over which the integral of $\varepsilon(\boldsymbol{r})$ will result in a well-defined local field.

A quantity which is closely related conceptually to the local energy density is the local stress density (also known as the local stress tensor field), $\sigma_{\alpha\beta}(\boldsymbol{r})$, which is defined as any tensor field whose divergence is the vector force field [4–9]. Like $\varepsilon(\boldsymbol{r})$, $\sigma_{\alpha\beta}(\boldsymbol{r})$ is inherently non-unique in nature since it can be specified only up to the addition of the curl of an arbitrary tensor field (this leaves the force density, a physical observable, invariant). The stress tensor field results in the average macroscopic stress tensor (a 'global' property) when integrated over the volume of the supercell [8, 9]. The stress density is composed of two contributions [4–9]: one due to the momentum flux density arising from the kinetic energy of interacting electrons, and the other, called the configurational stress density, arising from the potential of interaction of the electrons and the nuclei. The first contribution is inherently quantum mechanical in nature, and the traditional approach for deriving expressions for it starts with the local momentum density operator and the Heisenberg equation of motion, and results in complicated operator expressions [7–9]. The configurational part of the stress density is defined in terms of the internal electric fields resulting from the nuclear and electronic distributions [4–9], in direct analogy with the Maxwell stress tensor of classical electromagnetism [10]. For very simple systems, explicit expressions for both the momentum flux density and configurational terms have been derived [5–7]. For instance, expressions for the stress tensor field in the H atom and H_2 molecule have been given by Feynman [5] and Deb and Bamzai [6], respectively. Folland [7] has derived formal operator expressions particularly suited to one-electron approximations, and has used these formal expressions to determine explicit forms for $\sigma_{\alpha\beta}(\boldsymbol{r})$ in the isolated Ne and Ar atoms [7] within the local density approximation (LDA) of density functional theory (DFT) and at the Hartree–Fock level of theory. Formal operator expressions for more complicated

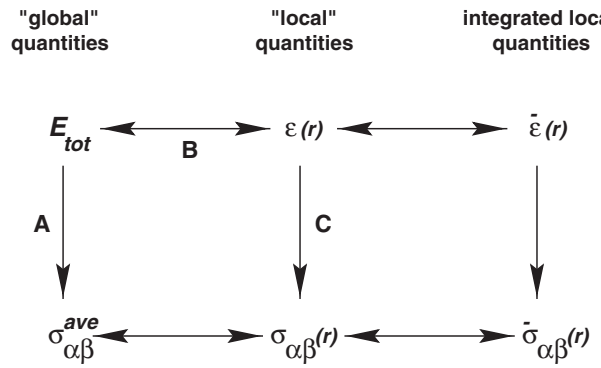

Figure 1. A schematic diagram of the relationships between the global (E_{tot}, $\sigma_{\alpha\beta}^{ave}$), the local ($\varepsilon(\boldsymbol{r})$, $\sigma_{\alpha\beta}(\boldsymbol{r})$) and the integrated local ($\bar{\varepsilon}(\boldsymbol{r})$, $\bar{\sigma}_{\alpha\beta}(\boldsymbol{r})$) quantities. The quantities at the bottom ($\sigma_{\alpha\beta}^{ave}$, $\sigma_{\alpha\beta}(\boldsymbol{r})$ and $\bar{\sigma}_{\alpha\beta}(\boldsymbol{r})$) are obtained by taking the strain derivatives of the respective quantities at the top (E_{tot}, $\varepsilon(\boldsymbol{r})$ and $\bar{\varepsilon}(\boldsymbol{r})$).

many-particle systems (many-atom clusters, periodic systems, systems with atomic cores represented by pseudopotentials) have also been derived [8, 9]; however, these expressions have proved too cumbersome for practical use. Here, we develop an alternative approach to the derivation of an explicit expression for the stress tensor field of a general periodic system to be used in plane-wave pseudopotential supercell calculations [2], within the LDA of DFT [11]. Rather than adopt the traditional equation of motion procedure which leads to operator expressions for $\sigma_{\alpha\beta}(\boldsymbol{r})$ [4–9], we derive an explicit analytic expression for $\sigma_{\alpha\beta}(\boldsymbol{r})$ by directly taking the strain derivative of the local energy density. Our procedure is schematically illustrated in figure 1. Since the average macroscopic stress is the strain derivative of the total energy per unit-cell volume [8, 12, 13] (denoted by path A in figure 1), the stress tensor field, $\sigma_{\alpha\beta}(\boldsymbol{r})$, is evidently the strain derivative of $\varepsilon(\boldsymbol{r})$ (path C in figure 1). The derivation of an expression for the stress tensor field therefore depends crucially on our ability to define the energy density (path B in figure 1). In the present study, we use a modified form of the energy density proposed earlier by Chetty and Martin [1]. The new form for $\varepsilon(\boldsymbol{r})$, and the resulting $\sigma_{\alpha\beta}(\boldsymbol{r})$ facilitate direct contact with previously derived pseudopotential-based density functional expressions for the corresponding macroscopic observables: the total energy [2] and average macroscopic stress tensor [8, 12, 13], respectively.

As defined, $\varepsilon(\boldsymbol{r})$ and $\sigma_{\alpha\beta}(\boldsymbol{r})$ exhibit variations on the scale of sub-atomic dimensions (the latter is referred to as the *microscopic* stress density in the literature [4–9], reflecting this property). Their corresponding (unique) macroscopic analogues are the integrals of these microscopic quantities over the volume of the unit cell. In order to bridge the length-scale gap between these two extremes, we define the integrated local fields, $\bar{\varepsilon}(\boldsymbol{r})$ and $\bar{\sigma}_{\alpha\beta}(\boldsymbol{r})$, as integrals of $\varepsilon(\boldsymbol{r})$ and $\sigma_{\alpha\beta}(\boldsymbol{r})$, respectively, over a Wigner–Seitz (WS) cell (or integral multiples of the WS cell). (The integrated local fields are also shown in figure 1 to complete the relationships between the global, local and integrated local quantities.) Thus, while $\varepsilon(\boldsymbol{r})$ and $\sigma_{\alpha\beta}(\boldsymbol{r})$ are the energy and stress densities at a point $\boldsymbol{r}$ in space, $\bar{\varepsilon}(\boldsymbol{r})$ and $\bar{\sigma}_{\alpha\beta}(\boldsymbol{r})$ are the corresponding properties averaged over a WS cell centred at the reference point $\boldsymbol{r}$. As a result, for defect-free periodic systems, $\bar{\varepsilon}(\boldsymbol{r})$ and $\bar{\sigma}_{\alpha\beta}(\boldsymbol{r})$ reduce to the corresponding macroscopic bulk quantities. In defect calculations using supercells much larger than the WS cell, the integrated local quantities capture the local effects due the defect in the neighbourhood of the defect, but far away from the defect, they recover their defect-free bulk values. To demonstrate the application of these local concepts to the microscopic characterization of defects, we consider two test cases: an

isolated vacancy in bulk Al, and an Al(001) surface. The surface calculation leads to some important observations regarding the potential use of $\bar{\sigma}_{\alpha\beta}(\boldsymbol{r})$ to help understand the driving force behind anomalous outward surface relaxations seen in some clean surfaces [14].

The paper is organized as follows. In section 2, we discuss the general considerations governing the construction of physically meaningful local fields. In section 3, we review a reformulation (derived earlier by Chetty and Martin [1]) of the usual reciprocal-space expression for the total energy [2]; this alternative formulation provides a more natural starting point for the construction of the local energy field, $\varepsilon(\boldsymbol{r})$. Expressions for $\varepsilon(\boldsymbol{r})$ and $\bar{\varepsilon}(\boldsymbol{r})$ are derived, and the approach of Chetty and Martin [1] is extended to treat more general defects; it is also shown that $\bar{\varepsilon}(\boldsymbol{r})$ exhibits the correct limiting behaviour in the defect-free case. In section 4, we give the expression for the average macroscopic stress tensor derived from the reformulated total energy expression of section 3; we then derive an expression for the non-unique microscopic symmetric stress tensor field, $\sigma_{\alpha\beta}(\boldsymbol{r})$, and discuss its properties. In section 5, we present results for defect-free bulk Al, bulk Al with a vacancy and a seven-layer Al(100) slab. We discuss implications and potential applications of the local fields concept in section 6 and conclude with a brief summary in section 7.

2. General considerations governing the construction of local fields

As mentioned in the Introduction, the local energy density, $\varepsilon(\boldsymbol{r})$, is required to satisfy the following important constraint:

$$E_{tot} = \int_{\Omega_{cell}} \varepsilon(\boldsymbol{r})\, \mathrm{d}^3\boldsymbol{r}, \tag{1}$$

where E_{tot} is the total energy per supercell of the system and Ω_{cell} is the volume of the periodic supercell. $\varepsilon(\boldsymbol{r})$ is thus a scalar quantity like the charge density, but unlike the latter, it is not a physical observable. Clearly, the construction of $\varepsilon(\boldsymbol{r})$ is possible only if each contribution to E_{tot} can be written as an integral of a local function in real space, so that each integrand can be identified as a separate and legitimate contribution to $\varepsilon(\boldsymbol{r})$. However, not all terms in the usual total energy expression within the pseudopotential approximation [2] are of this form. This problem is handled by reformulating the total energy expression (section 3.1), and defining an integrated local energy density, $\bar{\varepsilon}(\boldsymbol{r})$ (later in this section).

The density functional total energy (in Rydberg atomic units) within the LDA for a periodic array of ions (represented by non-local pseudopotentials) embedded in a charge-compensating valence electron gas is given by [2]

$$\begin{aligned} E_{tot} = &- \sum_{n\boldsymbol{k}} f_{n\boldsymbol{k}} \int \psi^*_{n\boldsymbol{k}}(\boldsymbol{r})\, \nabla^2 \psi_{n\boldsymbol{k}}(\boldsymbol{r})\, \mathrm{d}^3\boldsymbol{r} + \frac{1}{2} \int_{\Omega_{cell}} \int_{\Omega_{cell}} \frac{2\rho^e(\boldsymbol{r})\rho^e(\boldsymbol{r}')}{|\boldsymbol{r}-\boldsymbol{r}'|}\, \mathrm{d}^3\boldsymbol{r}\, \mathrm{d}^3\boldsymbol{r}' \\ &+ \int_{\Omega_{cell}} \epsilon_{XC}(\rho^e(\boldsymbol{r}))\rho^e(\boldsymbol{r})\, \mathrm{d}^3\boldsymbol{r} + \int \sum_{n\boldsymbol{k}jl} \psi^*_{n\boldsymbol{k}}(\boldsymbol{r}) V^{nl}_{jl}(|\boldsymbol{r}-\boldsymbol{\tau}_j|) \wp_l \psi_{n\boldsymbol{k}}(\boldsymbol{r})\, \mathrm{d}^3\boldsymbol{r} \\ &+ \int_{\Omega_{cell}} \sum_j V^{loc}_{ion,j}(|\boldsymbol{r}-\boldsymbol{\tau}_j|)\rho^e(\boldsymbol{r})\, \mathrm{d}^3\boldsymbol{r} + \frac{1}{2} \sum_{j \neq j'} \frac{2Z_j Z_{j'}}{|\boldsymbol{\tau}_j - \boldsymbol{\tau}_{j'}|}, \end{aligned} \tag{2}$$

where $f_{n\boldsymbol{k}}$ and $\psi_{n\boldsymbol{k}}(\boldsymbol{r})$ are the occupation number and the Kohn–Sham wavefunction, respectively, for the nth band and first-Brillouin-zone (IBZ) wavevector $\boldsymbol{k}$, $\rho^e(\boldsymbol{r})$ is the valence electronic charge density, $\epsilon_{XC}(\rho^e(\boldsymbol{r}))$ is the exchange–correlation energy per electron of a homogeneous electron gas of density ρ^e, $V^{nl}_{jl}(r)$ is the lth component of the non-local part of the pseudopotential of ion j, $\wp_l$ is the projection operator for angular momentum l, $V^{loc}_{ion,j}(r)$ is the local part of the pseudopotential of ion j and Z_j is the valence charge of ion j at location $\boldsymbol{\tau}_j$.

The total non-interacting electronic kinetic energy is given by the first term. There are two possible choices for the kinetic energy component of the energy density [1,15]: the symmetric ($-\sum_{nk} f_{nk}|\nabla\psi_{nk}(\boldsymbol{r})|^2\,\mathrm{d}^3\boldsymbol{r}$) and the antisymmetric ($-\sum_{nk} f_{nk}\psi^*_{nk}(\boldsymbol{r})\,\nabla^2\psi_{nk}(\boldsymbol{r})\,\mathrm{d}^3\boldsymbol{r}$) forms, both of which integrate to the total electronic kinetic energy. In most situations the two forms are equivalent. However, in some pathological cases $\nabla^2\psi_{nk}(\boldsymbol{r})$ may have singularities even if $\psi_{nk}(\boldsymbol{r})$ is well behaved [1]; in such cases, the antisymmetric form of the kinetic energy density may be undefined at some places. Although most situations of interest to us will not exhibit such pathological features, we follow Chetty and Martin [1] in choosing the symmetric form.

The electronic electrostatic energy, the exchange–correlation energy and the electron–pseudopotential interaction energy for the local part of the pseudopotential (the second, third and the fifth terms of equation (2), respectively) naturally adapt themselves to the construction of energy density components, since they can each be expressed as an integral of the product of $\rho^e(\boldsymbol{r})$ with a local function $v(\boldsymbol{r})$, where $v(\boldsymbol{r})$ is the electronic Hartree potential, the exchange–correlation energy per electron and the local part of the ionic pseudopotential, respectively, in the three cases. Thus, contributions to $\varepsilon(\boldsymbol{r})$ for these cases are of the form $\rho^e(\boldsymbol{r})v(\boldsymbol{r})$ (or $\sum_{\boldsymbol{G},\boldsymbol{G}'}\rho^*(\boldsymbol{G})\mathrm{e}^{-\mathrm{i}\boldsymbol{G}\cdot\boldsymbol{r}}v(\boldsymbol{G}')\mathrm{e}^{\mathrm{i}\boldsymbol{G}'\cdot\boldsymbol{r}}$ in reciprocal space, where $\boldsymbol{G}$ and $\boldsymbol{G}'$ are reciprocal-lattice vectors). Chetty and Martin [1], on the other hand, chose a Maxwell form [10] for the electrostatic component of the energy density. While our form for the electrostatic component of the energy density is motivated by the fact that it enables us to make direct contact with the corresponding term in the density functional total energy expression, Chetty and Martin [1] use the analogy with classical electromagnetic theory where the (Maxwell) energy density due to a distribution of charges is expressed in terms of the electric field due to the charge distribution. (The Maxwell energy density for the electrostatic component is given by $\boldsymbol{\zeta}^2(\boldsymbol{r})/(8\pi)$, where the electric field vector $\boldsymbol{\zeta}(\boldsymbol{r})$ is the gradient of the Hartree potential, $\boldsymbol{\zeta}(\boldsymbol{r}) = -\nabla\int\rho^e(\boldsymbol{r})/|\boldsymbol{r}-\boldsymbol{r}'|\,\mathrm{d}^3\boldsymbol{r}$.) Both the choices result in the total electrostatic energy when integrated over the volume of the supercell; the difference between the two forms is thus an example of a gauge term which integrates to zero over an appropriate integration volume.

The non-local component of the total energy due to the pseudopotential (the fourth term in equation (2)) does not adapt itself naturally to our procedure for constructing $\varepsilon(\boldsymbol{r})$. We have therefore chosen to calculate this term for each ionic site j, and to localize it as a Dirac delta function at that site. That is, we rewrite the fourth term in equation (2) as $\int_{\Omega_{cell}}\sum_j E^{nl}_j\delta(\boldsymbol{r}-\boldsymbol{\tau}_j)\,\mathrm{d}^3\boldsymbol{r}$, where

$$E^{nl}_j = \int\sum_{nkl}\psi^*_{nk}(\boldsymbol{r})V^{nl}_{jl}(|\boldsymbol{r}-\boldsymbol{\tau}_j|)\wp_l\psi_{nk}(\boldsymbol{r})\,\mathrm{d}^3\boldsymbol{r}. \tag{3}$$

E^{nl}_j is thus the non-local pseudopotential contribution to the total energy due to ion j and we identify $\sum_j E^{nl}_j\delta(\boldsymbol{r}-\boldsymbol{\tau}_j)$ as the total non-local pseudopotential contribution to $\varepsilon(\boldsymbol{r})$. By localizing an inherently non-local component, we are introducing an error in $\varepsilon(\boldsymbol{r})$. However, later in this section we will show that the physically significant quantity useful in analysing defects is actually $\bar{\varepsilon}(\boldsymbol{r})$, which is the integral of $\varepsilon(\boldsymbol{r})$ over a volume that is an integer multiple of the WS cell. Since the non-locality due to the pseudopotential is restricted to lying within a WS cell, $\bar{\varepsilon}(\boldsymbol{r})$ is insensitive to the details of the localization procedure.

The last term in equation (2) is the electrostatic ion–ion interaction energy, which, like the non-local part of the pseudopotential contribution to the total energy, cannot be expressed immediately as an integrated quantity. Nor is a localization procedure similar to the one adopted to write down the non-local pseudopotential contribution to $\varepsilon(\boldsymbol{r})$ justified, due to the long-range nature of this interaction. Hence, we regroup terms in the total energy expression of equation (2) (section 3.1) so that the ion–ion interaction component can be naturally incorporated into $\varepsilon(\boldsymbol{r})$.

Although the non-unique $\varepsilon(\boldsymbol{r})$ is interesting in its own right, it is only its integral (whenever unique) that is of physical significance. Equation (1) provides a specific instance where this quantity should integrate to a unique physical observable. By virtue of the form of our expression for $\varepsilon(\boldsymbol{r})$, it is also possible to define a family of integrals over volumes *smaller* than Ω_{cell} that yield meaningful integrated local energy fields. Intuition dictates that the smallest such integration volume in periodic solid-state systems is that of the WS cell, Ω_{WS}, for the system under consideration. Therefore, we define an integrated energy density of the form

$$\bar{\varepsilon}(\boldsymbol{r}) \equiv \frac{1}{\Omega_{subcell}} \int_{\Omega_{subcell}} \varepsilon(\boldsymbol{r} - \boldsymbol{r}')\, \mathrm{d}^3\boldsymbol{r}', \tag{4}$$

where $\bar{\varepsilon}(\boldsymbol{r})$ is the local energy density integrated over a volume, $\Omega_{subcell}$, which is an integral multiple of the WS cell volume centred around the reference point $\boldsymbol{r}$. For a defect-free periodic bulk system (even with a supercell larger than the WS cell), $\bar{\varepsilon}(\boldsymbol{r})$ should be a unique, constant function in space (equal to E_{tot}/Ω_{cell}); we give a formal proof of this statement in section 3.3. For systems with defects, deviations from constancy will provide information about the local nature and environment of the defect. At long range, we expect $\bar{\varepsilon}(\boldsymbol{r})$ to recover its constant bulk value.

We now turn our attention to the local stress tensor field, which is formally defined, by analogy with classical elasticity theory [16], as any tensor field whose divergence is the vector force field [4–9]:

$$\sum_{\alpha} \nabla_{\alpha} \sigma_{\alpha\beta}(\boldsymbol{r}) = f_{\beta}(\boldsymbol{r}), \tag{5}$$

where $\sigma_{\alpha\beta}(\boldsymbol{r})$ ($\alpha, \beta = x, y, z$) is the non-unique stress tensor field and $\boldsymbol{f}(\boldsymbol{r})$ is the vector force field. As with $\varepsilon(\boldsymbol{r})$, the integral of $\sigma_{\alpha\beta}(\boldsymbol{r})$ over the entire volume of the periodic supercell results in a physical observable—in this case, the average macroscopic stress tensor [8, 9]:

$$\sigma_{\alpha\beta}^{ave} = \frac{1}{\Omega_{cell}} \int_{\Omega_{cell}} \sigma_{\alpha\beta}(\boldsymbol{r})\, \mathrm{d}^3\boldsymbol{r}. \tag{6}$$

We derive an expression for $\sigma_{\alpha\beta}(\boldsymbol{r})$ in section 4.2 by taking the strain derivative of $\varepsilon(\boldsymbol{r})$. By analogy with equation (4), we define an integrated stress tensor field, $\bar{\sigma}_{\alpha\beta}(\boldsymbol{r})$, which is related to $\bar{\varepsilon}(\boldsymbol{r})$ as follows:

$$\begin{aligned} \bar{\sigma}_{\alpha\beta}(\boldsymbol{r}) = \frac{1}{(2-\delta_{\alpha\beta})} \frac{\delta\bar{\varepsilon}(\boldsymbol{r})}{\delta\epsilon_{\alpha\beta}} &= \frac{1}{\Omega_{subcell}(2-\delta_{\alpha\beta})} \int_{\Omega_{subcell}} \frac{\delta\varepsilon(\boldsymbol{r}-\boldsymbol{r}')}{\delta\epsilon_{\alpha\beta}}\, \mathrm{d}^3\boldsymbol{r}' \\ &= \frac{1}{\Omega_{subcell}} \int_{\Omega_{subcell}} \sigma_{\alpha\beta}(\boldsymbol{r}-\boldsymbol{r}')\, \mathrm{d}^3\boldsymbol{r}', \end{aligned} \tag{7}$$

where $\epsilon_{\alpha\beta}$ is a symmetric, uniform strain and the last equality defines the microscopic stress tensor field in the present treatment; the $(2 - \delta_{\alpha\beta})$ factor arises from the fact that we are interested in the symmetric stress tensor [12]. The relationships between the macroscopic ('global'), the local and the integrated local quantities are shown schematically in figure 1.

3. The local energy density

3.1. Reformulation of the reciprocal-space representation of the total energy

As discussed in the previous section, the construction of $\varepsilon(\boldsymbol{r})$ requires a reformulation of the usual expression for the total energy (equation (2)) [2] by changing the manner in which terms are grouped [1]. This new form will facilitate the construction of the local energy field in an intuitive manner, particularly with respect to the ion–ion interaction contribution, while

properly treating the $\boldsymbol{G} = 0$ divergent terms. Such a reformulation has been performed earlier by Chetty and Martin [1], and will be reviewed in this subsection.

In the new form, the electrostatic electronic Hartree contribution and the ion–ion interactions are treated together, with an associated modification to the local part of the pseudopotential contribution to the total energy. The electronic kinetic energy, exchange–correlation and non-local pseudopotential contributions to the total energy (first, third and fifth terms in equation (2)) in the present form are identical to those in the conventional form [2].

We start with the conventional expression for the total energy, in which the ion–ion interaction contribution (last term in equation (2)) is computed via the Ewald technique [2,17]. The Ewald method involves adding and subtracting a fictitious charge distribution composed of Gaussians at each ionic site j (with net charge Z_j), and performing two rapidly convergent sums, one in real space and the other in reciprocal space. The real- and reciprocal-space representations of the fictitious charge distribution are given by

$$\rho^n(\boldsymbol{r}) = \sum_j \frac{Z_j}{\eta^3}\left(\frac{2}{\pi}\right)^{3/2} \mathrm{e}^{-2\eta^2|\boldsymbol{r}-\boldsymbol{\tau}_j|^2} \tag{8}$$

$$\rho^n(\boldsymbol{G}) = \frac{1}{\Omega_{cell}} \mathrm{e}^{-G^2/8\eta^2} \sum_j Z_j \mathrm{e}^{-\mathrm{i}\boldsymbol{G}\cdot\boldsymbol{\tau}_j}, \tag{9}$$

where η is the Gaussian width. In the present study, by carefully choosing η, we make the real-space summation negligibly small. The reciprocal-space Ewald summation is composed of two terms [2, 17], one of which ($4\pi\Omega_{cell}\sum_{\boldsymbol{G}}|\rho^n(\boldsymbol{G})|^2/|\boldsymbol{G}|^2$) is identical in form to the reciprocal-space electronic Hartree contribution to the total energy. The other is $\sum_j E_j^{self}$, which effectively subtracts out the energy of the self-interaction of the ionic charges with each other. E_j^{self} is given by [2, 17]

$$E_j^{self} = -\frac{2\eta}{\sqrt{\pi}} Z_j^2. \tag{10}$$

By defining the total charge density, $\rho^t(\boldsymbol{r})$, as

$$\rho^t(\boldsymbol{r}) = \rho^e(\boldsymbol{r}) - \rho^n(\boldsymbol{r}), \tag{11}$$

we find that the total electrostatic contribution to the total energy is given by

$$E_{es} = \begin{cases} 4\pi\Omega_{cell}{\sum_{\boldsymbol{G}}}' \dfrac{|\rho^t(\boldsymbol{G})|^2}{|\boldsymbol{G}|^2} + \displaystyle\sum_j E_j^{self} & \text{(reciprocal space)} \\ \dfrac{1}{2}\displaystyle\int_{\Omega_{cell}}\int_{\Omega_{cell}} \frac{2\rho^t(\boldsymbol{r})\rho^t(\boldsymbol{r}')}{|\boldsymbol{r}-\boldsymbol{r}'|}\,\mathrm{d}^3\boldsymbol{r}\,\mathrm{d}^3\boldsymbol{r}' + \displaystyle\sum_j E_j^{self} & \text{(real space)} \end{cases}$$

where the prime indicates that the $\boldsymbol{G} = 0$ term is excluded from the summation; note that due to the definition of $\rho^t(\boldsymbol{r})$, the $\boldsymbol{G} = 0$ contribution is zero. The above expressions thus account for both the electron–electron and ion–ion interactions correctly, provided that the width of the Gaussian functions is chosen appropriately; however, it also contains a cross term, representing the interaction between the electrons and the Gaussian-broadened ions. Since the electron–ion interaction must be treated using pseudopotentials, the cross term which is part of the above expression is subtracted out while including the contribution due to the local part of the pseudopotential (fifth term in equation (12) below).

With all these modifications, the total energy per supercell within the LDA becomes

$$E_{tot} = -\sum_{n\boldsymbol{k}} \int \psi^*_{n\boldsymbol{k}}(\boldsymbol{r})\,\nabla^2\psi_{n\boldsymbol{k}}(\boldsymbol{r})\,\mathrm{d}^3\boldsymbol{r} + \frac{1}{2}\int_{\Omega_{cell}}\int_{\Omega_{cell}} \frac{2\rho^t(\boldsymbol{r})\rho^t(\boldsymbol{r}')}{|\boldsymbol{r}-\boldsymbol{r}'|}\,\mathrm{d}^3\boldsymbol{r}\,\mathrm{d}^3\boldsymbol{r}' + \int_{\Omega_{cell}} \epsilon_{XC}(\boldsymbol{r})\rho^e(\boldsymbol{r})\,\mathrm{d}^3\boldsymbol{r} + \sum_j E^{nl}_j + \int_{\Omega_{cell}} \left(\sum_j V^{loc}_{ion,j}(|\boldsymbol{r}-\boldsymbol{\tau}_j|) + \int_{\Omega_{cell}} \frac{2\rho^n(\boldsymbol{r}')}{|\boldsymbol{r}-\boldsymbol{r}'|}\,\mathrm{d}^3\boldsymbol{r}'\right)\rho^e(\boldsymbol{r})\,\mathrm{d}^3\boldsymbol{r} + \sum_j E^{self}_j \tag{12}$$

in real space and

$$E_{tot} = \sum_{n\boldsymbol{k}\boldsymbol{G}} f_{n\boldsymbol{k}}|c_{n\boldsymbol{k}}(\boldsymbol{G})|^2|\boldsymbol{k}+\boldsymbol{G}|^2 + 4\pi\Omega_{cell}{\sum_{\boldsymbol{G}}}' \frac{|\rho^t(\boldsymbol{G})|^2}{|\boldsymbol{G}|^2} + \Omega_{cell}\sum_{\boldsymbol{G}} \epsilon_{XC}(\boldsymbol{G})\rho^{e*}(\boldsymbol{G}) + \sum_j E^{nl}_j + \Omega_{cell}{\sum_{\boldsymbol{G}}}' \rho^{e*}(\boldsymbol{G})\left(\sum_j \mathrm{e}^{-\mathrm{i}\boldsymbol{G}\cdot\boldsymbol{\tau}_j} V^{loc}_{ion,j}(\boldsymbol{G}) + 8\pi\frac{\rho^n(\boldsymbol{G})}{|\boldsymbol{G}|^2}\right) + \sum_{jj'}\left(\alpha_j Z_{j'} - \frac{\pi Z_j Z_{j'}}{\eta^2\Omega_{cell}}\right) + \sum_j E^{self}_j \tag{13}$$

in reciprocal space. In equation (13), the $c_{n\boldsymbol{k}}(\boldsymbol{G})$'s denote the coefficients in the plane-wave expansion of the wavefunction [2], and $\epsilon_{XC}(\boldsymbol{G})$, $\rho^e(\boldsymbol{G})$ and $V^{loc}_{ion,j}(\boldsymbol{G})$ are the reciprocal-space representations of the exchange–correlation energy per electron, the valence electronic charge density and the local part of the pseudopotential of ion j, respectively. The fifth term in equation (13) does not include the $\boldsymbol{G}=0$ contribution, which is separated out explicitly as the sixth term. α_j is the usual repulsive term given by [2]

$$\alpha_j = \frac{1}{\Omega_{cell}}\int\left(V^{loc}_{ion,j}(r) + \frac{2Z_j}{r}\right)\mathrm{d}^3\boldsymbol{r}. \tag{14}$$

The reciprocal-space representation of E^{nl}_j is given by [2]

$$E^{nl}_j = \sum_{n\boldsymbol{k}} f_{n\boldsymbol{k}} \sum_{lm}\left[\sum_{\boldsymbol{G}} c^*_{n\boldsymbol{k}}(\boldsymbol{G})\mathrm{e}^{-\mathrm{i}\boldsymbol{G}\cdot\boldsymbol{\tau}_j} V^{nl}_{lj}(\boldsymbol{q})Y_{lm}(\hat{\boldsymbol{q}})\right]\left[\sum_{\boldsymbol{G}'} c_{n\boldsymbol{k}}(\boldsymbol{G}')\mathrm{e}^{\mathrm{i}\boldsymbol{G}'\cdot\boldsymbol{\tau}_j} V^{nl}_{lj}(\boldsymbol{q}')Y^*_{lm}(\hat{\boldsymbol{q}}')\right] \tag{15}$$

with

$$V^{nl}_{lj}(\boldsymbol{q}) = \frac{4\pi}{\sqrt{\Omega_{cell}}}\int_0^\infty j_l(qr)V^{nl}_{jl}(r)r^2\,\mathrm{d}r, \tag{16}$$

where $\boldsymbol{q} = \boldsymbol{k}+\boldsymbol{G}$, the Y_{lm} are spherical harmonics and the j_l are spherical Bessel functions.

3.2. Construction of $\varepsilon(\boldsymbol{r})$

Using the considerations outlined in section 2 and the reformulated total energy expressions of section 3.1 (equations (12) and (13)), we can now write down our form for the local energy field as follows, in close correspondence with equation (13) (such that each term in the following expression, when integrated over Ω_{cell}, results in the corresponding terms in equation (13)):

$$\varepsilon(\boldsymbol{r}) = T(\boldsymbol{r}) + E^H(\boldsymbol{r}) + E_{XC}(\boldsymbol{r}) + \sum_j E^{nl}_j\delta(\boldsymbol{r}-\boldsymbol{\tau}_j) + E^{loc}(\boldsymbol{r}) + \sum_j E^{self}_j\delta(\boldsymbol{r}-\boldsymbol{\tau}_j), \tag{17}$$

where

$$T(\boldsymbol{r}) = \frac{1}{\Omega_{cell}} \sum_{n\boldsymbol{k}} f_{n\boldsymbol{k}} \left| \sum_{\boldsymbol{G}} c_{n\boldsymbol{k}}(\boldsymbol{G})(\boldsymbol{k}+\boldsymbol{G}) \mathrm{e}^{\mathrm{i}\boldsymbol{G}\cdot\boldsymbol{r}} \right|^2, \tag{18}$$

$$E^H(\boldsymbol{r}) = 4\pi \sum_{\boldsymbol{G}} \rho^{t*}(\boldsymbol{G}) \mathrm{e}^{-\mathrm{i}\boldsymbol{G}\cdot\boldsymbol{r}} {\sum_{\boldsymbol{G}'}}' \frac{\rho^t(\boldsymbol{G}')}{|\boldsymbol{G}'|^2} \mathrm{e}^{\mathrm{i}\boldsymbol{G}'\cdot\boldsymbol{r}}, \tag{19}$$

$$E_{XC}(\boldsymbol{r}) = \sum_{\boldsymbol{G}} \rho^{e*}(\boldsymbol{G}) \mathrm{e}^{-\mathrm{i}\boldsymbol{G}\cdot\boldsymbol{r}} \sum_{\boldsymbol{G}'} \epsilon_{XC}(\boldsymbol{G}') \mathrm{e}^{\mathrm{i}\boldsymbol{G}'\cdot\boldsymbol{r}} \tag{20}$$

and

$$E^{loc}(\boldsymbol{r}) = \sum_{\boldsymbol{G}} \rho^{e*}(\boldsymbol{G}) \mathrm{e}^{-\mathrm{i}\boldsymbol{G}\cdot\boldsymbol{r}} {\sum_{\boldsymbol{G}'}}' \left[\sum_j \mathrm{e}^{-\mathrm{i}\boldsymbol{G}'\cdot\boldsymbol{\tau}_j} V^{loc}_{ion,j}(\boldsymbol{G}') + 8\pi \frac{\rho^n(\boldsymbol{G}')}{|\boldsymbol{G}'|^2} \right] \mathrm{e}^{\mathrm{i}\boldsymbol{G}'\cdot\boldsymbol{r}}$$
$$+ \rho^{e*}(\boldsymbol{G}) \mathrm{e}^{-\mathrm{i}\boldsymbol{G}\cdot\boldsymbol{r}} \sum_j \left(\alpha_j - \frac{\pi Z_j}{\eta^2 \Omega_{cell}} \right). \tag{21}$$

Note that we have chosen to localize the ionic self-interaction contribution due to ion j as a Dirac delta function at site j. This choice is entirely arbitrary; as in the case of the non-local pseudopotential term, the non-uniqueness of $\varepsilon(\boldsymbol{r})$ and the definition of $\bar{\varepsilon}(\boldsymbol{r})$ allow such a procedure.

As discussed earlier, Chetty and Martin [1] specifically chose to use the Maxwell form for $E^H(\boldsymbol{r})$ [1] in their derivation of $\varepsilon(\boldsymbol{r})$; all other components of $\varepsilon(\boldsymbol{r})$ are identical to ours. This use of what amounts to two different theoretical prescriptions in computing their Hartree and local pseudopotential contributions means that exact cancellation of the electron–fictitious ion cross term, which is part of the Hartree term, does not occur in their case. However, as we are ultimately interested in the integrated local energy density $\bar{\varepsilon}(\boldsymbol{r})$, and because the uncancelled contribution in their case integrates to zero within the integration volumes chosen here, this choice of one form versus another for $E^H(\boldsymbol{r})$ is not crucial.

Each of the terms in equation (17) can be efficiently calculated using fast Fourier transform (FFT) techniques; calculation of $\varepsilon(\boldsymbol{r})$ takes just a fraction of the time required for a single SCF iteration.

3.3. Properties of $\varepsilon(\boldsymbol{r})$

Equation (4) defines the integrated local energy density, $\bar{\varepsilon}(\boldsymbol{r})$. In this section, we show that the local energy density of a defect-free system (with a supercell larger than the WS cell) when integrated over $\Omega_{subcell}$ (or, equivalently, Ω_{WS}), results in a gauge-independent, unique, constant quantity, characteristic of the bulk material.

Consider a supercell calculation in which the supercell is composed of an integral number of WS cells. Reciprocal-space quantities are based on the set of vectors $\{\boldsymbol{G}\}$, where $\boldsymbol{G} = l\boldsymbol{b}_1 + m\boldsymbol{b}_2 + n\boldsymbol{b}_3$ are the reciprocal-lattice vectors, $\boldsymbol{b}_1$, $\boldsymbol{b}_2$ and $\boldsymbol{b}_3$ are the reciprocal-lattice basis vectors for our supercell, and l, m and n are integers. An independent calculation based on the WS cell will use the set of vectors $\{\boldsymbol{g}\}$, with $\boldsymbol{g} = l\boldsymbol{b}'_1 + m\boldsymbol{b}'_2 + n\boldsymbol{b}'_3$, $\boldsymbol{b}'_1$, $\boldsymbol{b}'_2$ and $\boldsymbol{b}'_3$ being the reciprocal-lattice basis vectors for the WS cell, l, m and n again being integers. Clearly, $\{\boldsymbol{g}\}$ is a subset of $\{\boldsymbol{G}\}$.

Each of the terms in the above expression for the local energy density, except for the non-local and the self-interaction terms, is of the form $\sum_{\boldsymbol{G}} a^*(\boldsymbol{G}) \mathrm{e}^{-\mathrm{i}\boldsymbol{G}\cdot\boldsymbol{r}} {\sum_{\boldsymbol{G}}}' b(\boldsymbol{G}') \mathrm{e}^{-\mathrm{i}\boldsymbol{G}'\cdot\boldsymbol{r}}$, whose integral over the volume of the WS cell yields

$$\mathcal{I} = \int_{\Omega_{WS}} \sum_{\boldsymbol{G}} a^*(\boldsymbol{G}) \mathrm{e}^{-\mathrm{i}\boldsymbol{G}\cdot\boldsymbol{r}} \sum_{\boldsymbol{G}'} b(\boldsymbol{G}') \mathrm{e}^{\mathrm{i}\boldsymbol{G}'\cdot\boldsymbol{r}} \, \mathrm{d}^3\boldsymbol{r} = \sum_{\boldsymbol{G},\boldsymbol{G}'} a^*(\boldsymbol{G}) b(\boldsymbol{G}') \int_{\Omega_{WS}} \mathrm{e}^{-\mathrm{i}(\boldsymbol{G}-\boldsymbol{G}')\cdot\boldsymbol{r}} \, \mathrm{d}^3\boldsymbol{r}. \tag{22}$$

Clearly, $a(\boldsymbol{r})$ and $b(\boldsymbol{r})$ (which are the real-space quantities corresponding to $a(\boldsymbol{G})$ and $b(\boldsymbol{G})$, respectively) are periodic functions, with the periodic volumes being the WS cell in the present case. Therefore, all Fourier components involving $\boldsymbol{G}$-vectors not in the set $\{\boldsymbol{g}\}$ are zero. Thus,

$$\mathcal{I} = \sum_{\boldsymbol{g},\boldsymbol{g}'} a^*(\boldsymbol{g}) b(\boldsymbol{g}') \int_{\Omega_{WS}} \mathrm{e}^{-\mathrm{i}(\boldsymbol{g}-\boldsymbol{g}')\cdot\boldsymbol{r}}\,\mathrm{d}\boldsymbol{r} \tag{23}$$

$$= \Omega_{WS} \sum_{\boldsymbol{g}} a^*(\boldsymbol{g}) b(\boldsymbol{g}). \tag{24}$$

The above expression is simply the general term (not including the non-local and ionic self-interaction terms) in the total energy expression for an independent calculation based on the WS cell itself; the non-local and ionic self-interaction terms in the local energy density expression also integrate to the corresponding terms in the total energy expression for a calculation based on the WS cell. Thus, we have shown that the local energy density resulting from a defect-free supercell calculation integrated over its WS cell results in the total energy of the WS cell (E_{tot}^{WS}), and the integrated local energy density itself is equal to E_{tot}^{WS}/Ω_{WS} ($=E_{tot}/\Omega_{cell}$).

The same conclusions hold when the integration volume is any integral multiple of the WS cell volume. As mentioned earlier, in the presence of a defect, local characteristics specific to the defect will be captured in $\bar{\varepsilon}(\boldsymbol{r})$, and it may be desirable to integrate $\varepsilon(\boldsymbol{r})$ over volumes larger than the WS cell volume, depending on the extent of the defect.

In the present study, the integration volume for the determination of local quantities was chosen to be the cubic Bravais unit cell (consisting of four WS cells). Thus, the integrated local energy density was determined as

$$\bar{\varepsilon}(\boldsymbol{r}) = \frac{1}{a_0^3} \int_{-a_0/2}^{a_0/2} \int_{-a_0/2}^{a_0/2} \int_{-a_0/2}^{a_0/2} \varepsilon(\boldsymbol{r}-\boldsymbol{r}')\,\mathrm{d}x'\,\mathrm{d}y'\,\mathrm{d}z', \tag{25}$$

where a_0 is the equilibrium lattice constant. The corresponding reciprocal-space representation is given by

$$\bar{\varepsilon}(\boldsymbol{G}) = \frac{\sin(G_x a_0/2)}{G_x a_0/2} \frac{\sin(G_y a_0/2)}{G_y a_0/2} \frac{\sin(G_z a_0/2)}{G_z a_0/2} \varepsilon(\boldsymbol{G}), \tag{26}$$

where $\varepsilon(\boldsymbol{G})$ is the local energy density in reciprocal space. The above expression can be used to efficiently calculate $\bar{\varepsilon}(\boldsymbol{r})$ using FFT techniques.

4. The local stress tensor field

4.1. The average macroscopic stress tensor

Expressions for the average macroscopic stress tensor, a physical observable and a global quantity, defined as the differential of the total energy with respect to a uniform, symmetric strain, $\epsilon_{\alpha\beta}$, have been obtained by previous authors [8, 12, 13]. Here, for completeness (and to compare with the integral of $\sigma_{\alpha\beta}(\boldsymbol{r})$ later), we provide an alternative expression for $\sigma_{\alpha\beta}^{ave}$ derived by starting from the reformulated total energy expression of section 3.1 (equation (13)):

$$\begin{aligned}\sigma_{\alpha\beta}^{ave} &= \frac{1}{\Omega_{cell}(2-\delta_{\alpha\beta})} \frac{\delta E_{tot}}{\delta \epsilon_{\alpha\beta}} \\ &= -2 \sum_{n\boldsymbol{k}\boldsymbol{G}} f_{n\boldsymbol{k}} |c_{n\boldsymbol{k}}(\boldsymbol{G})|^2 q_\alpha q_\beta \\ &\quad + 4\pi {\sum_{\boldsymbol{G}}}' \frac{|\rho^t(\boldsymbol{G})|^2}{G^2} \left(\frac{2G_\alpha G_\beta}{G^2} - \delta_{\alpha\beta} \right) - 4\pi {\sum_{\boldsymbol{G}}}' \frac{\rho^{t*}(\boldsymbol{G})}{G^2} \frac{\delta \rho^t(\boldsymbol{G})}{\delta \boldsymbol{G}} \left(\frac{2G_\alpha G_\beta}{G^2} \right)\end{aligned}$$

$$+\delta_{\alpha\beta}\sum_{\boldsymbol{G}}(\epsilon_{XC}(\boldsymbol{G})-\mu_{XC}(\boldsymbol{G}))\rho^{e*}(\boldsymbol{G})+\frac{1}{(2-\delta_{\alpha\beta})}\frac{\delta E^{nl}_{pp}}{\delta\epsilon_{\alpha\beta}}$$
$$-\sum_{j\boldsymbol{G}}{}'\mathrm{e}^{-\mathrm{i}\boldsymbol{G}\cdot\boldsymbol{\tau}_j}\left(\frac{\delta V^{loc}_{ion,j}(\boldsymbol{G})}{\delta\boldsymbol{G}}\frac{G_\alpha G_\beta}{G}+V^{loc}_{ion,j}(\boldsymbol{G})\delta_{\alpha\beta}\right)\rho^{e*}(\boldsymbol{G})$$
$$-\sum_{\boldsymbol{G}}{}'\rho^{e*}(\boldsymbol{G})\left(\left(\frac{\delta\rho^n(\boldsymbol{G})}{\delta\boldsymbol{G}}-\frac{\rho^n(\boldsymbol{G})}{G}\right)\frac{G_\alpha G_\beta}{G^3}+\frac{\rho^n(\boldsymbol{G})}{G^2}\delta_{\alpha\beta}\right)$$
$$+\left(\sum_j\frac{\pi Z_j}{\Omega^2_{cell}\eta^2}-\frac{\alpha_j}{\Omega_{cell}}\right)\left(\sum_j Z_j\right)\delta_{\alpha\beta}, \tag{27}$$

where

$$\frac{1}{(2-\delta_{\alpha\beta})}\frac{\delta E^{nl}_{pp}}{\delta\epsilon_{\alpha\beta}}=-\sum_{n\boldsymbol{k}j}f_{n\boldsymbol{k}}\sum_{lm}\frac{1}{M_l}\left[\sum_{\boldsymbol{G}}c^*_{n\boldsymbol{k}}(\boldsymbol{G})\mathrm{e}^{-\mathrm{i}\boldsymbol{G}\cdot\boldsymbol{\tau}_j}v_{lj}(\boldsymbol{q})Y_{lm}(\hat{\boldsymbol{q}})\right]$$
$$\times\left[\sum_{\boldsymbol{G}}c_{n\boldsymbol{k}}(\boldsymbol{G})\mathrm{e}^{\mathrm{i}\boldsymbol{G}\cdot\boldsymbol{\tau}_j}v_{lj}(\boldsymbol{q})\left(q_\alpha\frac{\delta Y^*_{lm}(\hat{\boldsymbol{q}})}{\delta q_\beta}\right)\right.$$
$$\left.+\frac{1}{2}\delta_{\alpha\beta}v_{lj}(\boldsymbol{q})Y^*_{lm}(\hat{\boldsymbol{q}})-\bar{v}_{lj}(\boldsymbol{q})Y^*_{lm}(\hat{\boldsymbol{q}})\frac{q_\alpha q_\beta}{|\boldsymbol{q}|^2}\right]+\text{c.c.} \tag{28}$$

with

$$\bar{v}_{lj}(\boldsymbol{q})=\frac{4\pi}{\sqrt{\Omega_{cell}}}\frac{1}{2l+1}\int_0^\infty[(l+1)j_{l+1}(|\boldsymbol{q}\cdot\boldsymbol{r}|)-j_{l-1}(|\boldsymbol{q}\cdot\boldsymbol{r}|)]v_{lj}(r)r^3\,\mathrm{d}r \tag{29}$$

and

$$\frac{\delta V^{loc}_{ion,j}(\boldsymbol{G})}{\delta\boldsymbol{G}}=-\frac{4\pi}{\Omega_{cell}}\int_0^\infty r^3 j_1(|\boldsymbol{G}\cdot\boldsymbol{r}|)V^{loc}_{ion,j}(r)\,\mathrm{d}r. \tag{30}$$

In determining the strain derivatives, we have used the relation [12]

$$\frac{1}{(2-\delta_{\alpha\beta})}\frac{\delta f(\boldsymbol{G})}{\delta\epsilon_{\alpha\beta}}=-\left(\frac{\delta f(\boldsymbol{G})}{\delta\boldsymbol{G}}\frac{G_\alpha G_\beta}{G}+f(\boldsymbol{G})\delta_{\alpha\beta}\right). \tag{31}$$

The average macroscopic pressure, p, due to a uniform, symmetric strain is related to the trace of the average macroscopic stress tensor as follows:

$$p=-\tfrac{1}{3}(\sigma_{11}+\sigma_{22}+\sigma_{33}). \tag{32}$$

4.2. Construction of $\sigma_{\alpha\beta}(\boldsymbol{r})$

The local stress tensor field defined in equation (5) can be obtained by term-by-term differentiation with respect to a uniform, symmetric strain $\epsilon_{\alpha\beta}$ of the local energy density:

$$\sigma_{\alpha\beta}(\boldsymbol{r})=\sigma^T_{\alpha\beta}(\boldsymbol{r})+\sigma^H_{\alpha\beta}(\boldsymbol{r})+\sigma^{XC}_{\alpha\beta}(\boldsymbol{r})+\sigma^{nl}_j(\boldsymbol{r})+\sigma^{loc}_{\alpha\beta}(\boldsymbol{r}), \tag{33}$$

where

$$\sigma^T_{\alpha\beta}(\boldsymbol{r})=-2\sum_{n\boldsymbol{k}}f_{n\boldsymbol{k}}\sum_{\boldsymbol{G}}c^*_{n\boldsymbol{k}}(\boldsymbol{G})\mathrm{e}^{-\mathrm{i}\boldsymbol{G}\cdot\boldsymbol{r}}q_\alpha\sum_{\boldsymbol{G}'}c_{n\boldsymbol{k}}(\boldsymbol{G}')\mathrm{e}^{\mathrm{i}\boldsymbol{G}'\cdot\boldsymbol{r}}q_\beta, \tag{34}$$

$$\sigma^H_{\alpha\beta}(\boldsymbol{r})=-4\pi\sum_{\boldsymbol{G}}\rho^{t*}(\boldsymbol{G})\mathrm{e}^{-\mathrm{i}\boldsymbol{G}\cdot\boldsymbol{r}}\sum_{\boldsymbol{G}'}{}'\frac{\rho^t(\boldsymbol{G}')\mathrm{e}^{\mathrm{i}\boldsymbol{G}'\cdot\boldsymbol{r}}}{G'^2}\delta_{\alpha\beta}$$
$$+4\pi\sum_{\boldsymbol{G}}\rho^{t*}(\boldsymbol{G})\mathrm{e}^{-\mathrm{i}\boldsymbol{G}\cdot\boldsymbol{r}}\sum_{\boldsymbol{G}'}{}'\frac{\rho^t(\boldsymbol{G}')\mathrm{e}^{\mathrm{i}\boldsymbol{G}'\cdot\boldsymbol{r}}}{G'^2}\left(\frac{2G'_\alpha G'_\beta}{G'^2}\right)$$

$$- 4\pi \sum_{G} \rho^{t*}(\boldsymbol{G}) \mathrm{e}^{-\mathrm{i}\boldsymbol{G}\cdot\boldsymbol{r}} \sum_{G'}{}' \frac{\delta\rho^{n}(\boldsymbol{G}')}{\delta \boldsymbol{G}'} \frac{\mathrm{e}^{\mathrm{i}\boldsymbol{G}'\cdot\boldsymbol{r}}}{G'^2} \left(\frac{G'_\alpha G'_\beta}{G'} \right)$$
$$- 4\pi \sum_{G} \frac{\delta\rho^{n*}(\boldsymbol{G})}{\delta \boldsymbol{G}} \mathrm{e}^{-\mathrm{i}\boldsymbol{G}\cdot\boldsymbol{r}} \left(\frac{G_\alpha G_\beta}{G} \right) \sum_{G'}{}' \frac{\rho^{t}(\boldsymbol{G}')\mathrm{e}^{\mathrm{i}\boldsymbol{G}'\cdot\boldsymbol{r}}}{G'^2} \tag{35}$$

with

$$\frac{\delta\rho^{n}(\boldsymbol{G})}{\delta \boldsymbol{G}} = -\frac{1}{\Omega_{cell}} \left(\frac{G}{4\eta^2} \right) \mathrm{e}^{-G^2/8\eta^2} \sum_{j} Z_j \mathrm{e}^{-\mathrm{i}\boldsymbol{G}'\cdot\boldsymbol{\tau}_j}, \tag{36}$$

$$\sigma^{XC}_{\alpha\beta}(\boldsymbol{r}) = \delta_{\alpha\beta} \sum_{G} \rho^{e*}(\boldsymbol{G}) \mathrm{e}^{-\mathrm{i}\boldsymbol{G}\cdot\boldsymbol{r}} \sum_{G'} (\epsilon_{XC}(\boldsymbol{G}') - \mu_{XC}(\boldsymbol{G}')) \mathrm{e}^{\mathrm{i}\boldsymbol{G}'\cdot\boldsymbol{r}}, \tag{37}$$

$$\sigma^{nl}_{j}(\boldsymbol{r}) = \frac{\delta(\boldsymbol{r} - \boldsymbol{\tau}_j)}{(2 - \delta_{\alpha\beta})} \frac{\delta E^{nl}_{pp}}{\delta \epsilon_{\alpha\beta}} \tag{38}$$

and

$$\sigma^{loc}_{\alpha\beta}(\boldsymbol{r}) = - \sum_{j} \sum_{G}{}' \rho^{e*}(\boldsymbol{G}) \mathrm{e}^{-\mathrm{i}\boldsymbol{G}\cdot\boldsymbol{r}} \sum_{G'} \mathrm{e}^{\mathrm{i}\boldsymbol{G}'\cdot\boldsymbol{r}} \mathrm{e}^{\mathrm{i}\boldsymbol{G}'\cdot\boldsymbol{\tau}_j} \left(\frac{\delta V^{loc}_{ion,j}(\boldsymbol{G}')}{\delta \boldsymbol{G}'} \frac{G'_\alpha G'_\beta}{G'} + V^{loc}_{ion,j}(\boldsymbol{G}') \delta_{\alpha\beta} \right)$$
$$- 8\pi \sum_{G}{}' \rho^{e*}(\boldsymbol{G}) \mathrm{e}^{-\mathrm{i}\boldsymbol{G}\cdot\boldsymbol{r}} \sum_{G'} \mathrm{e}^{\mathrm{i}\boldsymbol{G}'\cdot\boldsymbol{r}} \left(\frac{\delta\rho^{n}(\boldsymbol{G}')}{\delta \boldsymbol{G}'} \frac{G'_\alpha G'_\beta}{G'^3} + \frac{\rho^{n}(\boldsymbol{G})}{G'^2} \delta_{\alpha\beta} \right)$$
$$+ 8\pi \sum_{G}{}' \rho^{e*}(\boldsymbol{G}) \mathrm{e}^{-\mathrm{i}\boldsymbol{G}\cdot\boldsymbol{r}} \sum_{G'} \mathrm{e}^{\mathrm{i}\boldsymbol{G}'\cdot\boldsymbol{r}} \left(\rho^{n}(\boldsymbol{G}') \frac{G'_\alpha G'_\beta}{G'^4} \right)$$
$$- \rho^{e*}(\boldsymbol{G}) \mathrm{e}^{-\mathrm{i}\boldsymbol{G}\cdot\boldsymbol{r}} \sum_{j} \left(\alpha_j - \frac{\pi Z_j}{\eta^2 \Omega_{cell}} \right) \delta_{\alpha\beta}. \tag{39}$$

It can be verified that $\sigma_{\alpha\beta}(\boldsymbol{r})$, when integrated over Ω_{cell}, results in the average macroscopic stress, $\sigma^{ave}_{\alpha\beta}$ (equation (27)).

4.3. Properties of $\sigma_{\alpha\beta}(\boldsymbol{r})$

The integrated stress tensor field, $\bar{\sigma}_{\alpha\beta}(\boldsymbol{r})$, is defined by equation (7). For defect-free systems subjected to a uniform strain, $\bar{\sigma}_{\alpha\beta}(\boldsymbol{r})$ is a constant function in space equal to the average macroscopic stress tensor, $\sigma^{ave}_{\alpha\beta}$. Defects introduce non-uniform strains, and in such cases $\bar{\sigma}_{\alpha\beta}(\boldsymbol{r})$ describes the local stress concentrations.

As in the calculation of $\bar{\varepsilon}(\boldsymbol{r})$, we use the cubic Bravais unit cell for the determination of the stress fields as well, with real- and reciprocal-space expressions for $\bar{\sigma}_{\alpha\beta}$ analogous to equations (25) and (26), respectively. In the present study, we focus on the integrated hydrostatic pressure field, $\bar{p}(\boldsymbol{r})$, which is related to the trace of the stress tensor field:

$$\bar{p}(\boldsymbol{r}) = -\tfrac{1}{3}(\bar{\sigma}_{11}(\boldsymbol{r}) + \bar{\sigma}_{22}(\boldsymbol{r}) + \bar{\sigma}_{33}(\boldsymbol{r})). \tag{40}$$

5. Results

In this section, we first present total energy results for defect-free bulk Al at equilibrium. We then focus on two examples of defected Al: bulk Al with an isolated vacancy, and a Al(001) surface, and examine the local energy and stress fields set up in these systems due to the defects, using the methods outlined in sections 3 and 4.

The electronic ground state for these systems was determined self-consistently using the Teter–Payne–Allan preconditioned conjugate gradient method [18] through the solution

of the Kohn–Sham single-particle equations. A norm-conserving non-local pseudopotential, transformed using the Kleinman–Bylander technique [19], was used to describe the Al cores. For the equilibrium bulk calculations (one atom per unit cell), 28 'special' $\boldsymbol{k}$-points were used to sample quantities within the irreducible wedge of the IBZ; 20 special $\boldsymbol{k}$-points within the IBZ were used for the vacancy calculation (31 atoms per unit cell) and 40 special $\boldsymbol{k}$-points were used for the Al(100) slab calculation (14 atoms per unit cell). All results reported here were well converged for the above choices of Brillouin zone meshes and a plane-wave cut-off energy of 16 Ryd.

5.1. Equilibrium bulk Al

Bulk Al exists as an fcc structure. The ground state of the system is obtained by minimizing the total energy per atom of the fcc structure with respect to the lattice constant, and the ground state properties are determined by fitting the theoretical values of energy and volume to an integrated equation of state [20] (figure 2(a)). We calculate the equilibrium lattice constant and bulk modulus to be 7.48 au and 85.3 GPa, respectively, the former being about 1.6% higher and the latter about 5% lower than experimental determinations [21, 22]. The deviation of the calculated properties from the observed ones are consistent with previous LDA results for bulk Al [23]. In figure 2(b), the average macroscopic pressure values calculated directly from first principles using equation (32) at a series of values of the lattice constant centred about the equilibrium are compared with the pressures estimated using the integrated equation of state [20]; as can be seen, the two curves are in excellent agreement.

5.2. Isolated vacancy in bulk Al

To demonstrate the utility of the integrated local quantities defined earlier, we consider bulk fcc Al with a point defect, modelled using a 32-site cubic supercell with one of the sites vacant. Figure 3 displays the valence charge density profile on a (001) plane for this supercell, with the vacancy at the centre of the plane. Not surprisingly, there is an accumulation of electronic charge at the bond centres, and depletion elsewhere, with the depletion most pronounced in the vicinity of the vacancy. We calculate the unrelaxed vacancy formation energy to be 0.82 eV, in excellent agreement with the results of a recent calculation using similar methods and supercell [24].

Figure 4 shows the integrated energy density, $\bar{\varepsilon}(\boldsymbol{r})$, along a (001) plane. At the boundaries of the supercell, the energy density takes on a value corresponding to defect-free equilibrium bulk Al, $\bar{\varepsilon}_{bulk}$ $(=E_{tot}^{WS}/\Omega_{WS})$, and in the vicinity of the vacancy, it increases from its bulk value with a shape consistent with the point symmetry at the vacancy. The energy density profile affords a means of partitioning space into a vacancy region (region of varying $\bar{\varepsilon}$) and a bulk region (region of constant $\bar{\varepsilon}$). The contribution to the vacancy formation energy comes entirely from the vacancy region; in fact, the integral of $\bar{\varepsilon}(\boldsymbol{r}) - \bar{\varepsilon}_{bulk}$ in the vacancy region yields a value of 0.82 eV in agreement with the vacancy formation energy calculated using total energy results. The increase in $\bar{\varepsilon}(\boldsymbol{r})$ close to the vacancy is to be expected since the vacancy region constitutes a region of coordination lower than the preferred 12-fold one in the bulk, and since the overall energy cost for creating a vacancy comes from this region. That $\bar{\varepsilon}(\boldsymbol{r})$ recovers its bulk value away from the vacancy indicates minimal interaction between the vacancy and its periodic images; this is a useful diagnostic for choosing supercells that are sufficiently large for the defect calculation.

Figure 5 portrays the integrated pressure field, $\bar{p}(\boldsymbol{r})$, along a (001) plane. The presence of the vacancy causes a low-pressure region in its neighbourhood and a high-pressure region

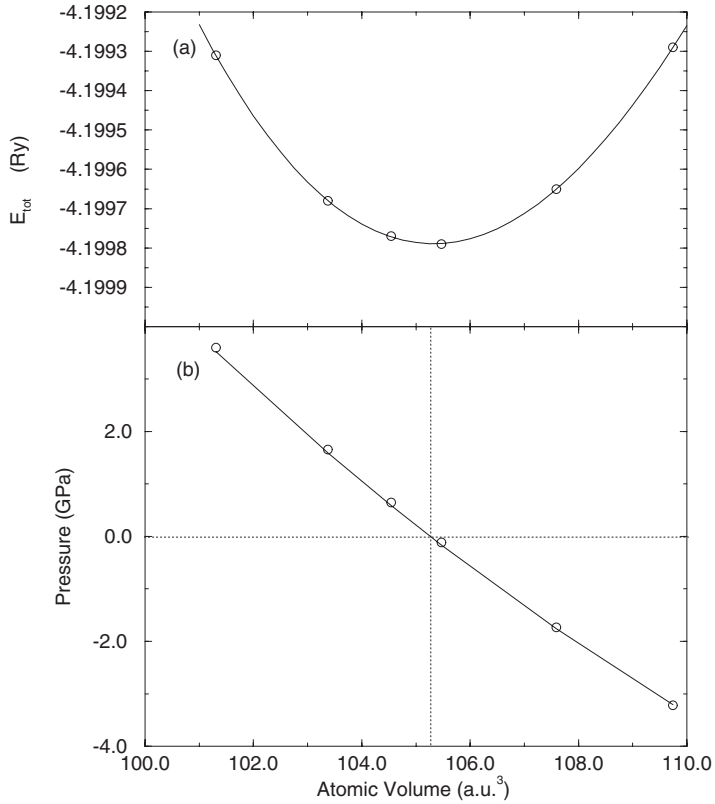

Figure 2. (a) Calculated total energies per WS cell for fcc bulk Al (open circles) are fitted to the Birch equation of state [20] (solid curve); (b) pressures calculated from the equation of state fit (solid line) of (a) are compared with those calculated directly from first principles (open circles).

just beyond the nearest-neighbour atoms. Inspection of the forces on the ionic cores also indicates a tendency for the atoms closest to the vacancy to relax towards the vacancy. Thus, the pressure field is consistent with the sense of the forces on the ionic cores, and also with the intuitive picture that atoms from a bulk-like region will want to 'flow' into a region of lower concentration and thereby relieve the pressure field that is generated due to the unrelaxed vacancy. The pressure field gradually goes to zero far away from the vacancy (characteristic of the equilibrium bulk), again indicating that the vacancies are well separated from each other.

5.3. Al(001) surface

We used a seven-layer Al(001) slab to model the Al(001) surface. The supercell in this case consisted of 14 atoms (two atoms per layer) and the periodic slabs were separated by three vacuum layers. The calculated surface energy for the unrelaxed slab is 69 meV Å^{-2}, which compares well with the experimental estimation of 71–74 meV Å^{-2} [25] averaged for low-surface-energy surfaces, and an earlier LDA result of 67 meV Å^{-2} for the Al(001) surface [26].

Since $\Omega_{subcell}$ is again the cubic Bravais unit cell, $\bar{\varepsilon}(\boldsymbol{r})$ and $\bar{\sigma}_{\alpha\beta}(\boldsymbol{r})$ are constant functions along planes parallel to the (001) surface, and vary only along directions perpendicular to the surface.

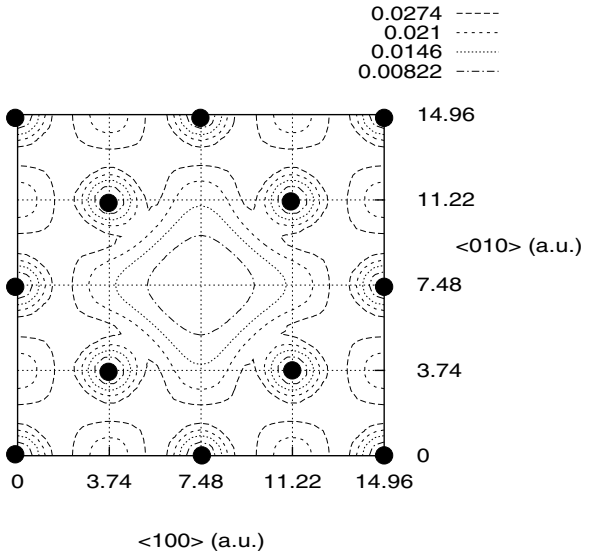

Figure 3. A contour plot at four levels of constant valence charge density (in au^{-3}) on the (001) plane for Al with an isolated vacancy (modelled with a 32-site cubic supercell). Atoms are shown as solid circles and the vacancy is at the centre of the plane shown.

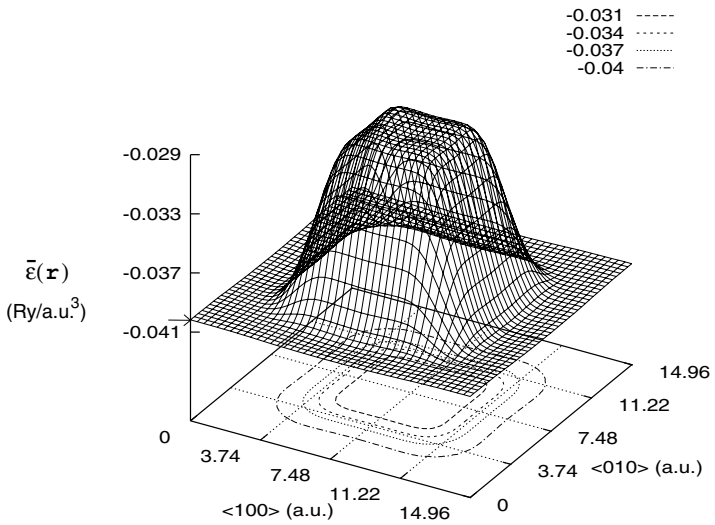

Figure 4. Integrated local energy density, $\bar{\varepsilon}(\boldsymbol{r})$ (in Ryd au^{-3}), along the (001) plane. $\bar{\varepsilon}(\boldsymbol{r})$ recovers its equilibrium bulk value (indicated by an arrow) away from the vacancy. A contour plot at four levels of constant $\bar{\varepsilon}(\boldsymbol{r})$ is also shown.

Figure 6 shows the $\bar{\varepsilon}(\boldsymbol{r})$ profile perpendicular to the (001) surface. As can be seen, $\bar{\varepsilon}(\boldsymbol{r})$ approaches its defect-free bulk value in the interior of the slab, increases from its bulk value in the vicinity of the free surface and approaches zero away from the surface in the vacuum region. Once again, we see that the supercell can be partitioned into bulk and surface regions. The integral of $\bar{\varepsilon}(\boldsymbol{r}) - \bar{\varepsilon}_{bulk}$ in the surface region yields the surface energy calculated above using total energy methods, indicating that the contribution to the surface formation energy

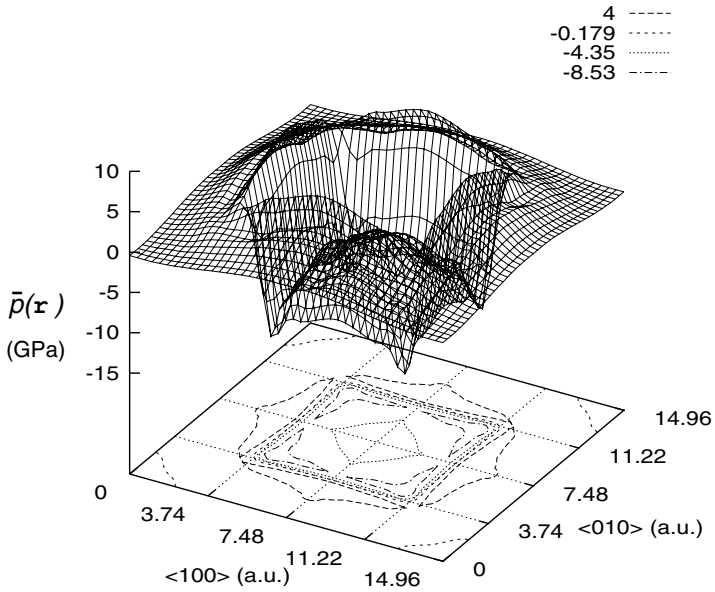

Figure 5. Integrated pressure field, $\bar{p}(\boldsymbol{r})$ (in GPa), along the (001) plane. $\bar{p}(\boldsymbol{r})$ recovers its equilibrium bulk value (namely, zero) away from the vacancy. A contour plot at four levels of constant $\bar{p}(\boldsymbol{r})$ is also shown.

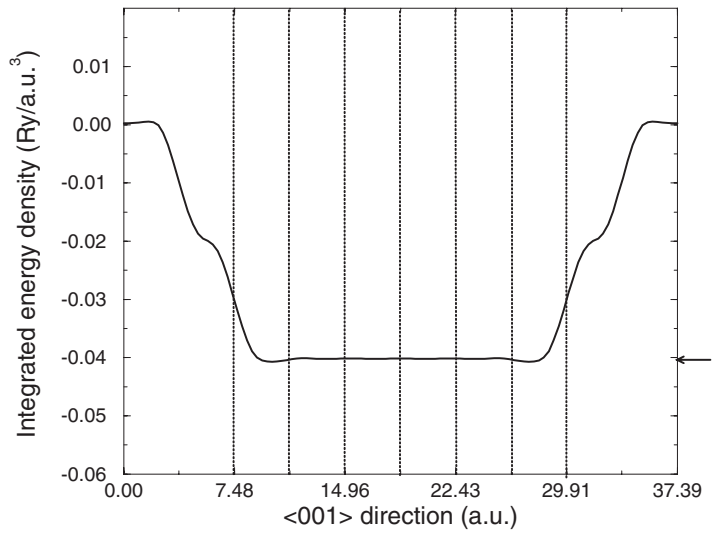

Figure 6. Integrated local energy density, $\bar{\varepsilon}(\boldsymbol{r})$, perpendicular to the (001) surface for a seven-layer Al(001) slab. Vertical dotted lines represent (001) layers and the arrow indicates $\bar{\varepsilon}$ corresponding to defect-free bulk Al.

comes entirely from the surface region. A point of inflection in the $\bar{\varepsilon}(\boldsymbol{r})$ profile can be seen about 3.7 au above the free surfaces. The origin of this feature is not clear, but it may be due to the electron gas that leaks out of the surface.

The integrated pressure field, $\bar{p}(\boldsymbol{r})$, along the $\langle 001 \rangle$ direction for the Al(001) slab is shown in figure 7. In the interior of the slab, $\bar{p}(\boldsymbol{r})$ takes on a value close to zero and characteristic of the equilibrium bulk, whereas in the neighbourhood of the surface, it deviates from the

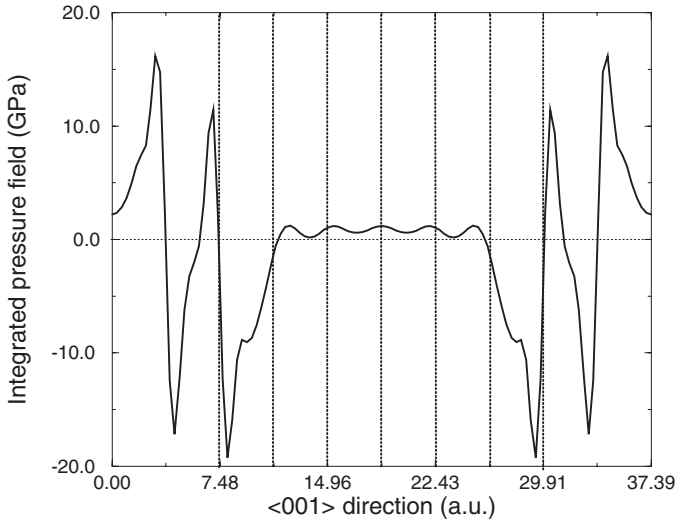

Figure 7. Integrated pressure, $\bar{p}(\boldsymbol{r})$, perpendicular to the (001) surface for a seven-layer Al(001) slab. Vertical dotted lines represent (001) layers.

near-zero value. Between the first and second surface layers, $\bar{p}(\boldsymbol{r})$ is negative and just outside the surface layer, it is positive, indicating a propensity for the surface layer to relax inward. However, in this case of defected Al (unlike in the case of an isolated vacancy in bulk Al), additional features can be seen in the integrated pressure field plot (figure 7), making the above conclusion of the surface relaxation tendency premature. In particular, interesting structure can be seen in the 'vacuum' region (the region on either sides of the slab) which consists of electron gas that has leaked out of the surface. We explore the implications of the integrated pressure field of figure 7 in greater detail in the following section. Inspection of the forces on the ionic cores indicates a tendency for negligible but *outward* relaxation; we calculate an outward force of 0.0004 eV au^{-1} on the surface layer, and an inward force of 0.046 eV au^{-1} on the second-layer atoms. This result is consistent with earlier theoretical calculations [26, 27] and with experiments [14].

6. Discussion

One of the underlying motivations for the present study was to develop new theoretical tools for the practical analysis of results from first-principles total energy calculations. Ideally, these tools should provide an intuitive picture of the underlying quantum mechanical structure of the system, without appealing to a single-particle orbital picture that, from a formal standpoint, cannot be justified within ground state DFT [28]. As an illustration of this approach, we outline the application of the pressure field, or more generally, the stress tensor field, to the analysis of surface relaxations.

Inward or negligible relaxation of the outer layer of atoms in metallic surfaces is so prevalent that significant outward relaxation is considered anomalous [14]. This characteristic behaviour is most simply explained [29] in terms of satisfying the coordination requirements of the outer-layer atoms, which have low coordination compared to the bulk atoms. The outer-layer atoms therefore move inward toward the second-layer atoms in order to saturate their dangling bonds. Consistent with this idea, surfaces which display negligible relaxation tend

to be closely packed. Their atoms are already well coordinated along the surface plane, so the driving force for inward relaxation is minimal. An alternative rationale [29] for inward surface relaxation is provided by the Smoluchowski effect [30]. In this picture, electrons close to the surface seek to decrease their kinetic energy by reducing the curvature of their wavefunctions. The electrons move from directly above the surface atoms to the hollows between them, and thus closer to the surface. This forces the ionic cores to move closer to the bulk as well.

Clearly, if these effects were the only factors governing surface relaxation, large outward relaxations would never occur. For this reason, experimental results supporting the existence of large outward relaxations have excited considerable theoretical interest. In some cases, mechanisms based on first-principles calculations have been proposed to explain the experimental results [29], but these are necessarily system-specific and cannot provide an intuitive picture of competing effects in the general case. The present work suggests that the pressure field may provide an alternative means for analysing a broad class of surfaces and relaxations.

As an example, consider the Al(001) pressure field illustrated in figure 7. At first glance, the pressure field in the vicinity of the outer surface layer and the forces on the surface and second-layer atoms appear to indicate contrasting directions for the Al(001) surface relaxation. This apparent contradiction can be resolved, however, by noting that:

(i) in general, the direction of the force on an atom (which is part of a larger system) and the local pressure around the atom need not be consistent with each other; the net force on an atom may be zero, even though the atom experiences non-zero pressures or stresses locally[1], which is precisely the case here; and
(ii) a complete picture of the various factors leading to the net force on the surface atoms requires an examination of the pressure field not just in the immediate neighbourhood of the outer surface, but also in the vacuum region.

Consider the pressure field illustrated in figure 7. The integrated pressure at a point $\boldsymbol{r}$ is the microscopic pressure averaged over a cubic Bravais cell with lattice constant 7.48 au, and centred at the reference point $\boldsymbol{r}$. Therefore, $\bar{p}(\boldsymbol{r})$ for r between 0.00 and 3.74 au or between 33.66 and 37.40 au along the $\langle 001 \rangle$ direction involves integration volumes consisting purely of electron gas, and so is positive (clearly, particles with like charge enclosed in a volume exert an outward, or positive, pressure on the volume boundaries). However, in the region between 3.74 and 7.48 au or between 29.92 and 33.66 au, $\bar{p}(\boldsymbol{r})$ involves integration volumes consisting of the electron gas in the vacuum region as well as the positively charged surface layer atoms. The large negative integrated pressures observed in parts of these regions represent the electrostatic attraction between the two oppositely charged entities. This leads to a driving force for outward surface relaxation. On the other hand, positive values of $\bar{p}(\boldsymbol{r})$ just outside the surface layer and negative values in the region between the outer- and second-layer atoms represent the preference for inward relaxation of the outer-layer atoms in order to satisfy their coordinative unsaturation. The positive values of $\bar{p}(\boldsymbol{r})$ in the region between 3.74 and 7.48 au are also consistent with the Smoluchowski effect [30]. In the case of Al(001), the various driving forces for inward and outward relaxation are nearly in balance, leading to a very small net outward relaxation. For other surfaces, the relaxations resulting from these competing effects will be more dramatic.

In addition to aiding in understanding the driving forces underlying surface relaxations, the stress field concept has a number of other direct applications to materials theory. It can be used to study the mechanisms driving surface reconstructions [31], the stability of interfaces

[1] A good example of a system in which the net force on each atom is zero while the pressure (locally and globally) is non-zero is a periodic infinite solid subjected to a uniform isostatic strain.

and interphases, and the interplay between structure and chemistry at point, line and planar defects. Specific examples include the growth of thin films on substrates, polymer/metal adhesion, precipitation of new phases during a phase transformation and the effect of impurity segregation on the cohesion or embrittlement of grain boundaries.

Finally, the energy and stress tensor fields have exciting potential applications as starting points for the development of materials models bridging scales of length and time. For example, the energy density field provides an intuitive framework for treating a defect—be it a vacancy or a grain boundary or a dislocation—as a spatially and energetically well-characterized quasi-particle. This suggests the use of the energy field to construct interaction potentials for atomistic or meso-scale defect dynamics simulations. The first-principles stress field can likewise provide a link between microscopic and macroscopic length scales by serving as an input to continuum models of deformation and dislocation phenomena [32]. Traditionally, such models are based on elasticity theory [33], and consequently, breakdown occurs in regions of plastic deformation (e.g., dislocation cores). Detailed information about the stress fields in these regions, obtained using the methods described in this work, would bridge this gap, and provide the potential for significant improvements in the fidelity of continuum materials models.

7. Summary

We have proposed a new approach to the microscopic characterization of defects in periodic systems by defining spatially varying local fields. In particular, we have identified two quantities, the local energy density $\varepsilon(\boldsymbol{r})$ and the local stress density $\sigma_{\alpha\beta}(\boldsymbol{r})$, which yield the total energy and the average macroscopic tensor, respectively, when integrated over the volume of the entire supercell. Although inherently non-unique in nature, $\varepsilon(\boldsymbol{r})$ and $\sigma_{\alpha\beta}(\boldsymbol{r})$ provide meaningful results when integrated over specific volumes, resulting in the integrated quantities, $\bar{\varepsilon}(\boldsymbol{r})$ and $\bar{\sigma}_{\alpha\beta}(\boldsymbol{r})$, respectively. In the presence of a defect, $\bar{\varepsilon}(\boldsymbol{r})$ and $\bar{\sigma}_{\alpha\beta}(\boldsymbol{r})$ capture the local chemical variations associated with the disturbance of the crystalline environment, while far away from the defect, they recover their bulk values. These features are reflected in our results for the test cases of bulk Al with a vacancy and the Al(001) surface. We have also outlined potential applications of these local concepts to the characterization of surface relaxations and in helping bridge phenomena occurring at different length scales.

Acknowledgments

I would like to thank the Albuquerque High Performance Computing Center (AHPCC), the National Center for Supercomputing Applications (NCSA), and the Maui High Performance Computing Center (MHPCC) for providing the computational resources used in this work. This research was supported by the National Science Foundation grant DMR-9520371. I would also like to thank Professor David Vanderbilt (Rutgers University) for helpful discussions, and Dr Susan Atlas for permission to use, and implement features (including the theory outlined in this paper) in, the total energy code VERNET.

References

[1] Chetty N and Martin R M 1992 *Phys. Rev.* B **45** 6074
Chetty N and Martin R M 1992 *Phys. Rev.* B **45** 6089
[2] Pickett W E 1989 *Comput. Phys. Rep.* **9** 115
[3] Chetty N and Martin R M 1991 *Phys. Rev.* B **44** 5568

[4] Schrödinger E 1927 *Ann. Phys., Lpz.* **82** 265
Pauli W 1958 1933 *Handbuch der Physik* Band XXIV, Part 1, vol 5 (Berlin: Springer) pp 83–272
[5] Feynman R P 1939 *BS Thesis* MIT
[6] Deb B M and Bamzai A S 1978 *Mol. Phys.* **35** 1349
Deb B M and Bamzai A S 1979 *Mol. Phys.* **38** 2069
[7] Folland N O 1986 *Phys. Rev.* B **34** 8296
Folland N O 1986 *Phys. Rev.* B **34** 8305
[8] Nielsen O H and Martin R M 1985 *Phys. Rev.* B **32** 3780 and references therein
Nielsen O H and Martin R M 1985 *Phys. Rev.* B **32** 3792
[9] Ziesche P, Gräfenstein J and Nielsen O H 1988 *Phys. Rev.* B **37** 8167
Godfrey M J 1988 *Phys. Rev.* B **37** 10 176 and references therein
[10] Jackson J D 1975 *Classical Electrodynamics* (New York: Wiley)
[11] Hohenberg P and Kohn W 1964 *Phys. Rev.* **136** B864
Kohn W and Sham L J 1965 *Phys. Rev.* **140** A1133
[12] Lee I-H, Lee S-G and Chang K J 1995 *Phys. Rev.* B **51** 14 697
[13] Bylander D M, Kleinman L and Lee S 1990 *Phys. Rev.* B **42** 1394
[14] Davis H L, Hannon J B, Ray K B and Plummer E W 1992 *Phys. Rev. Lett.* **68** 2632
Rodríguez A M, Bozzolo G and Ferrante J 1993 *Surf. Sci.* **289** 100 and references therein
[15] Slater J C 1937 *Phys. Rev.* **51** 846
[16] Landau L D and Lifshitz E M 1958 *Theory of Elasticity* vol 7 (New York: Pergamon)
[17] Tosi M P 1964 *Solid State Physics* vol 16, ed H Ehrenreich, F Seitz and D Turnbull (New York: Academic) p 1
[18] Teter M P, Payne M C and Allan D C 1989 *Phys. Rev.* B **40** 12 255
[19] Hamman D R 1989 *Phys. Rev.* B **40** 2980
Kleinman L and Bylander D M 1982 *Phys. Rev. Lett.* **48** 1425
[20] Birch F 1952 *J. Geophys. Res.* **57** 227
[21] Wyckoff R W G *Crystal Structures* 2nd edn, vol 1 (New York: Academic) p 10
[22] Simmons G and Wang H *Single Crystal Elastic Constants* (Cambridge, MA: MIT Press) p 233
[23] Lam P K and Cohen M L 1981 *Phys. Rev.* B **24** 4224 and references therein
[24] Chetty N, Weinert M, Rahman T S and Davenport J W 1995 *Phys. Rev.* B **52** 6313
[25] Tyson W R and Miller W A 1977 *Surf. Sci.* **62** 267
[26] Bohnen K-P and Ho K-M 1988 *Surf. Sci.* **207** 105
[27] Feibelman P J 1988 *Phys. Rev.* B **38** 1849
[28] See, for example,
Dreizler R M and Gross E K U 1990 *Density Functional Theory* (New York: Springer)
[29] Feibelman P J 1992 *Phys. Rev.* B **46** 2532
Wright A F, Feibelman P J and Atlas S R 1994 *Surf. Sci.* **302** 215
[30] Smoluchowski R 1941 *Phys. Rev.* **60** 661
Finnis M W and Heine V 1974 *J. Phys. F: Met. Phys.* **4** L37
[31] Vanderbilt D 1987 *Phys. Rev. Lett.* **59** 1456
Meade R D and Vanderbilt D 1991 *The Structure of Surfaces* vol 3, ed S Y Tong, M A Van Hove, K Takayanagi and X Xide (Berlin: Springer) p 4
Meade R D and Vanderbilt D 1990 *The Physics of Semiconductors* ed E M Anastassakis and J D Joannopoulos (Singapore: World Scientific) p 123
[32] Tadmor E B, Ortiz M and Phillips R 1996 *Phil. Mag.* A **73** 1529
[33] Hirth J P and Lothe J 1968 *Theory of Dislocations* (New York: McGraw-Hill)